

**Fig. 4.** Ligand-induced structural changes in  $\beta A$  in comparison with those of  $\alpha A$  (from CD11b). (A) Superposition, in stereo, of the  $\alpha V\beta 3$ -Mn (gray) and  $\alpha V\beta 3$ -RGD-Mn (red) structures. The superposition is based on the  $C\alpha$  atoms of the central  $\beta$ -sheet [43 atoms per structure; root mean square deviation (RMSD), 0.42 Å]. Residues of  $\alpha V\beta 3$ -RGD-Mn with a distance of more than 1.5 Å to corresponding residues of  $\alpha V\beta 3$ -Mn are shown with thicker red lines. The major structural changes in  $\beta A$  involve helices  $\alpha 1$ ,  $\alpha 1'$ ,  $\alpha 2$ , the F- $\alpha 7$  loop, and the ligand-specificity region. (B) Magnified view of the rearrangements at the ligand-binding site in  $\beta A$ . Superposition of the propeller and  $\beta A$  domains of  $\alpha V\beta 3$ -Mn (gray) and  $\alpha V\beta 3$ -RGD-Mn ( $\alpha V$ , blue;  $\beta 3$ , red) is based on the  $C\alpha$  atoms of the  $\alpha V$

propeller domain. The directions of protein movements (including the 4 Å displacement of  $Mn^{2+}$  at ADMIDAS) are indicated by red arrows. This view differs from (A) by a rotation of 180° around a vertical axis. (C) Superposition, in stereo, of the "liganded" (red) and "unliganded" forms of  $\alpha A$  from the CD11b integrin. The metal ion sphere at MIDAS is in cyan. The superposition is based on the  $C\alpha$  atoms of the central  $\beta$ -sheet (43 atoms; RMSD = 0.43 Å). Residues of liganded  $\alpha A$  with a distance of more than 1.5 Å to corresponding residues of unliganded  $\alpha A$  are shown with thicker red lines. The major structural changes in  $\alpha A$  involve helices  $\alpha 1$ ,  $\alpha 7$ , the F- $\alpha 7$ , and E- $\alpha 6$  loops. Arrows (red) indicate the direction of the major protein movements in each case.

## Resolution of Lung Inflammation by CD44

Priit Teder,<sup>1</sup> R. William Vandivier,<sup>2</sup> Dianhua Jiang,<sup>1</sup> Jiurong Liang,<sup>1</sup> Lauren Cohn,<sup>1</sup> Ellen Puré,<sup>3</sup> Peter M. Henson,<sup>2</sup> Paul W. Noble<sup>1\*</sup>

Successful repair after tissue injury and inflammation requires resolution of the inflammatory response and removal of extracellular matrix breakdown products. We have examined whether the cell-surface adhesion molecule and hyaluronan receptor CD44 plays a role in resolving lung inflammation. CD44-deficient mice succumb to unremitting inflammation following noninfectious lung injury, characterized by impaired clearance of apoptotic neutrophils, persistent accumulation of hyaluronan fragments at the site of tissue injury, and impaired activation of transforming growth factor- $\beta_1$ . This phenotype was partially reversed by reconstitution with CD44<sup>+</sup> cells, thus demonstrating a critical role for this receptor in resolving lung inflammation.

The pathogenesis of pulmonary fibrosis typically exhibits overlapping phases of inflammation and deposition of matrix. Successful repair of tissue injury requires resolution of

the inflammatory phase. Recent evidence has suggested that this is an active process requiring the release of soluble mediators as well as interactions between these mediators and

cell-surface matrix binding proteins (1, 2). A paradigm has emerged that, following tissue injury, there is an influx of polymorphonuclear leukocytes (PMNs) that subsequently undergo apoptosis and must be removed from tissues to allow normal repair to occur. However, in vivo evidence for a relation between removal of apoptotic PMNs and matrix fragments and successful repair of injury has not been obtained.

CD44 is a transmembrane adhesion receptor and the major cell-surface receptor for the nonsulfated glycosaminoglycan hyaluronan (HA) (3). CD44 plays an important role in the clearance of HA and mediates cell-matrix interactions involved in tumor formation, metastasis and T cell extravasation (4–6). HA is present in all tissues in a high molecular weight (MW) form in excess of 10<sup>6</sup> daltons (7). At sites of inflammation and tissue injury low-MW HA species accumulate and have proinflammatory functions (8). We examined the role of CD44 in the resolution of lung

injury using CD44-deficient mice that lack all known CD44 isoforms and manifest no overt developmental phenotype (9).

Intratracheal administration of bleomycin has been widely used as a model to study the mechanisms of lung injury and repair (10). Inflammation of the alveolar interstitium is present in the first week, followed by the accumulation of extracellular matrix components. C57Bl/6 mice survive but develop patchy lung fibrosis after bleomycin treatment. In contrast, 75% of CD44-deficient mice died by day 14 (Fig. 1A). Within 24 hours after intratracheal injection of bleomycin, focal areas with cellular influx into the alveolar interstitium were equally apparent in wild-type and CD44-deficient animals. Progressive accumulation of PMNs and lymphocytes, with further thickening of alveolar sep-

tae, was observed in wild-type animals until day 7, followed by resolution of inflammatory cell infiltrates and fibrotic repair at day 14 (Fig. 1B). In contrast, CD44-deficient mice exhibited massive infiltration of inflammatory cells within alveolar interstitium until death by respiratory failure by day 14 (Fig. 1B). Histologic evidence of the persistence of lung inflammation was confirmed by cytological analysis of cells obtained in bronchoalveolar lavage (BAL) (10). The total cell numbers recovered by BAL were similar for wild-type and CD44-deficient mice at baseline. After bleomycin treatment, the total cell numbers peaked at day 5 in wild-type mice and declined until day 10. In contrast, the total cell numbers increased in the CD44-deficient animals until death (Fig. 1C). Substantial increases in PMNs, macrophages, and lymphocytes each contributed to the increase in total BAL counts (Fig. 1, D through F). We examined the expression of chemokines that might selectively recruit inflammatory cell populations to the site of tissue injury (8). We found that MCP-5, MIP-2, and CRG-2 mRNAs were all induced in lung tissue following bleomycin treatment. The chemokine expression abated in the wild-

type mice by day 7, but persisted in the CD44-deficient mice (Fig. 1G).

In order to examine the contribution of matrix turnover to the observed pathology we examined the localization of HA in lung tissue (11). At 7 days after bleomycin treatment, both wild-type and CD44-deficient animals demonstrated a similar increase in HA staining within the alveolar septae and alveolar macrophages. However, at day 14, HA accumulation persisted within the interstitium intermixed with inflammatory cells in the CD44-deficient animals compared to wild-type animals (Fig. 2A). Quantitation of HA content in lung tissue revealed that CD44-deficient mice demonstrated a similar increase as wild-type mice at day 7 after bleomycin treatment, but unlike the wild-type mice, HA content continued to rise until death (Fig. 2B). In the 25% of mice that survived beyond day 14, the HA content declines, indicating a relationship between HA clearance and survival.

Under physiologic conditions, HA equilibrium in the lung is maintained by mobilization to the lymphatic system, where most is degraded by the liver, and by local removal in the alveolar interstitium, primarily by alveolar macrophages (7). As a result, the baseline BAL fluid from wild-type and CD44-deficient animals contain minute amounts of HA. However, following bleomycin treatment HA levels in BAL fluid from CD44-deficient mice rose progressively, reaching  $2845 \pm 127$  ng/ml prior to death (12). This was significantly greater than the concentration of  $1812 \pm 165$  ng/ml observed in the wild-type animals measured at the same time point ( $P = 0.0008$ ). These data suggest that excessive accumulation of HA in BAL fluid causes respiratory compromise.

The accumulation of low-MW HA fragments occurs by a variety of mechanisms, including depolymerization by reactive oxygen species, enzymatic cleavage, and de novo biosynthesis (13–15). To investigate the role of CD44 in the clearance of HA fragments, we performed HA MW analysis on lung tissues from CD44-deficient and wild-type mice following bleomycin treatment (16). Wild-type mice demonstrated an accumulation of lower MW HA species (Fig. 2C). Following resolution of inflammation, there was a return to higher MW species. Although untreated CD44-deficient mice demonstrated a similar preponderance of high-MW species as the wild-type mice, four distinct MW peaks could be detected with an accumulation of smaller fragments not observed in the wild-type mice after bleomycin treatment (Fig. 2C). These data suggest that CD44 plays a critical role in HA homeostasis following lung injury, and this influences the recovery from pulmonary inflammation.

Apoptosis is considered to be a protective mechanism allowing removal of inflammatory

<sup>1</sup>Department of Medicine, Pulmonary and Critical Care Section, Yale University School of Medicine, New Haven, CT 06520, and VA Connecticut Healthcare System, West Haven, CT 06516, USA. <sup>2</sup>Department of Pediatrics, National Jewish Medical and Research Center, Denver, CO 80206, USA. <sup>3</sup>Wistar Institute, Philadelphia, PA 19104, and The Ludwig Institute for Cancer Research, New York, NY 10158, USA.

\*To whom correspondence should be addressed. E-mail: paul.noble@yale.edu

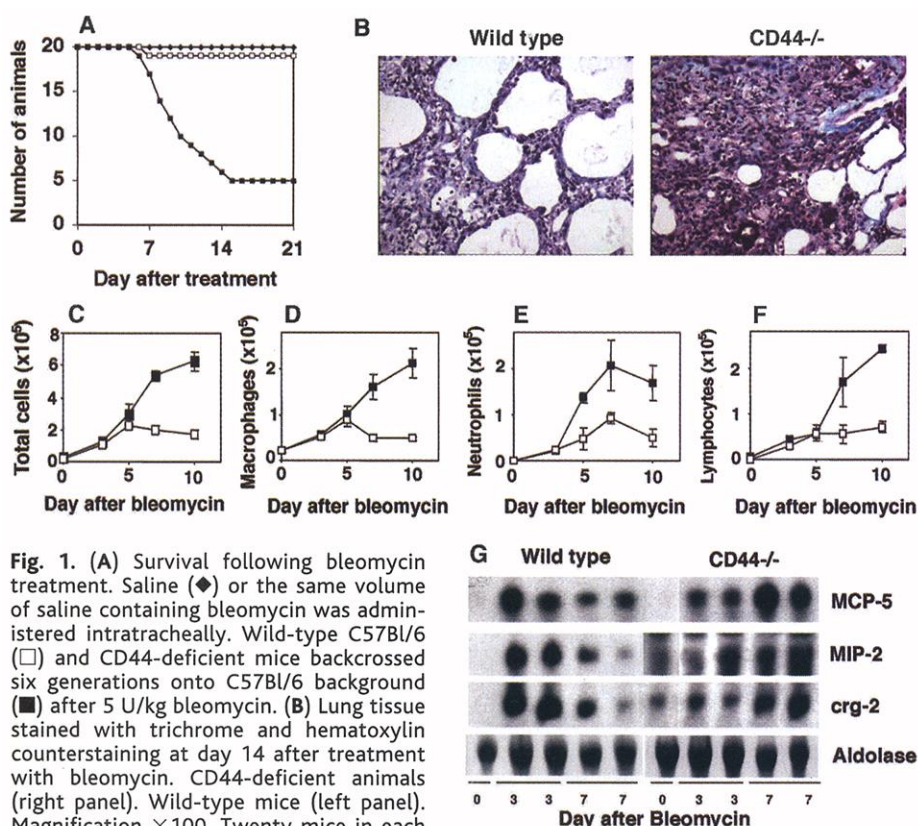


**Fig. 1.** (A) Survival following bleomycin treatment. Saline (◆) or the same volume of saline containing bleomycin was administered intratracheally. Wild-type C57Bl/6 (□) and CD44-deficient mice backcrossed six generations onto C57Bl/6 background (■) after 5 U/kg bleomycin. (B) Lung tissue stained with trichrome and hematoxylin counterstaining at day 14 after treatment with bleomycin. CD44-deficient animals (right panel). Wild-type mice (left panel). Magnification  $\times 100$ . Twenty mice in each group,  $n = 5$ . (C through F) Cellular profiles following bleomycin treatment. Wild-type (□) and CD44-deficient (■) animals. Results are from five animals in each group,  $n = 5$ . (G) Chemokine mRNA expression over time in wild-type (left panel) and CD44-deficient mice (right panel). Representative of three similar experiments.

cells before lysis, thus avoiding the release of immunogenic and potentially toxic intracellular contents. CD44 ligation on macrophages selectively promotes the uptake of apoptotic PMNs in vitro (17). Untreated wild-type and CD44-deficient mice exhibit only rare apoptotic cells in the lung interstitium (18). However, a 13-fold increase in the number of apoptotic cells was detected in the lung tissue of CD44-deficient mice compared to the wild type after bleomycin treatment (Fig. 3, A and B). In order to directly test if the accumulation of apoptotic inflammatory cells in CD44-deficient mice was due to impaired clearance, human PMNs made to undergo apoptosis in vitro, were instilled intratracheally into wild-type and CD44-deficient animals (19). Intratracheal lipopolysaccharide (20  $\mu$ g) was instilled 72 hours before the exogenous apoptotic PMNs to recruit inflammatory macrophages to the lung. CD44-deficient mice exhibited a marked defect in clearance of exogenous apoptotic PMNs from BAL fluid compared to wild-type mice (Fig. 3A). The phagocytic index (Fig. 3B) further supported an impaired ability of CD44-deficient macrophages to ingest apoptotic PMNs in vivo. Although CD44 does not appear to be a direct receptor for apoptotic cell recognition in vitro (17), it does appear from these observations to play a significant, though conceivably indirect, role in this process in vivo.

Recent evidence has suggested a fundamental role for transforming growth factor- $\beta_1$  (TGF- $\beta_1$ ) in down-regulating the inflammatory response while promoting fibrosis (2). In vitro studies have shown that phagocytosis of apoptotic PMNs provides an anti-inflammatory signal and promotes the release of TGF- $\beta_1$  (1). TGF- $\beta$ s are secreted in a latent form and are converted to an active form by a variety of mechanisms in vitro, but the in vivo mechanisms have not been elucidated. A novel mechanism has recently been suggested that involves a direct interaction between the metalloproteinase MMP-9 and CD44 resulting in the cleavage of latent TGF- $\beta$  (20). CD44-deficient animals demonstrated much lower levels of active TGF- $\beta_1$  in BAL fluid (21) relative to wild-type animals after bleomycin treatment (Fig. 3E). The decreased levels of active TGF- $\beta_1$  were not due to an absence of total TGF- $\beta_1$ , because acidification of the BAL fluid to activate latent TGF- $\beta_1$  demonstrated high concentrations of total (latent + active) TGF- $\beta_1$  from both CD44-deficient and wild-type animals (Fig. 3E). Thus, the inflammatory phenotype in CD44-deficient animals correlated strongly with reduced activation of latent TGF- $\beta_1$ .

CD44 is present on both hematopoietic cells as well as parenchymal cells such as epithelial cells and fibroblasts. In order to determine if hematopoietic CD44 was required to resolve lung inflammation, we reconstituted irradiated CD44-deficient mice

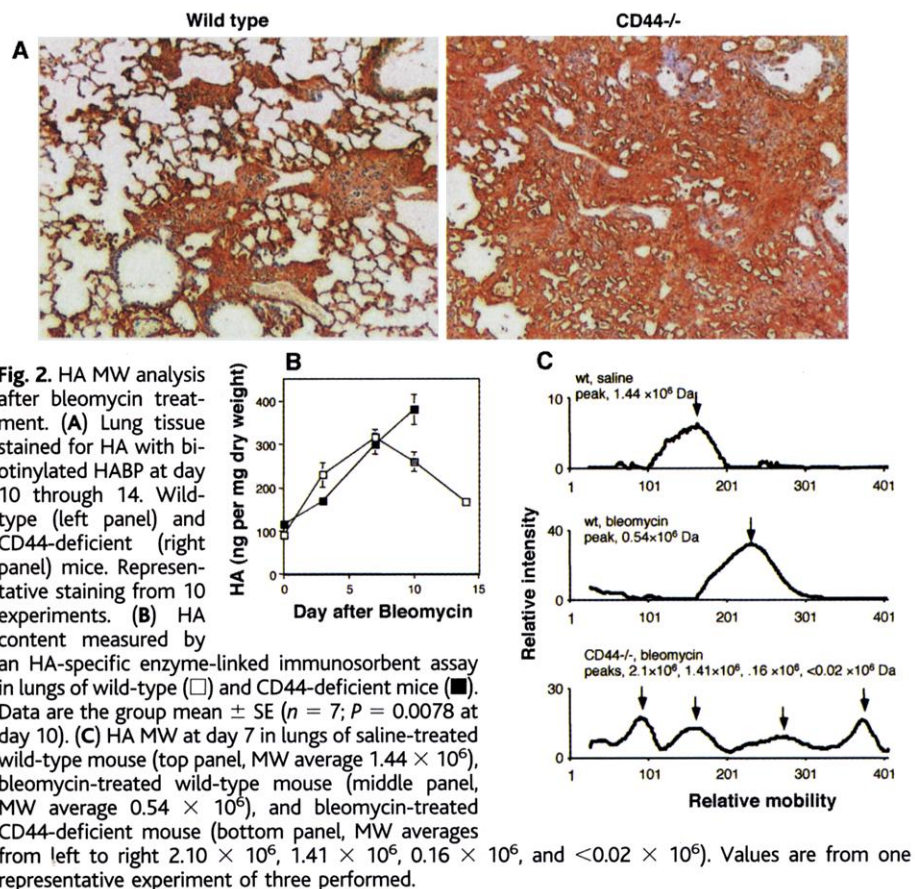


**Fig. 2.** HA MW analysis after bleomycin treatment. (A) Lung tissue stained for HA with biotinylated HABP at day 10 through 14. Wild-type (left panel) and CD44-deficient (right panel) mice. Representative staining from 10 experiments. (B) HA content measured by an HA-specific enzyme-linked immunosorbent assay in lungs of wild-type (□) and CD44-deficient mice (■). Data are the group mean  $\pm$  SE ( $n = 7$ ;  $P = 0.0078$  at day 10). (C) HA MW at day 7 in lungs of saline-treated wild-type mouse (top panel, MW average  $1.44 \times 10^6$ ), bleomycin-treated wild-type mouse (middle panel, MW average  $0.54 \times 10^6$ ), and bleomycin-treated CD44-deficient mouse (bottom panel, MW averages from left to right  $2.10 \times 10^6$ ,  $1.41 \times 10^6$ ,  $0.16 \times 10^6$ , and  $<0.02 \times 10^6$ ). Values are from one representative experiment of three performed.

**Fig. 3.** Clearance of apoptotic cells during lung inflammation. (A) Apoptotic cells (dark brown) in lungs of wild-type and CD44-deficient mice at day 7 after bleomycin. Magnification  $\times 100$ . (B) Quantitation of apoptotic cells after bleomycin treatment. Fifty fields were counted at a magnification of  $\times 400$  from four experiments. Results are mean  $\pm$  SE,  $n = 4$ . CD44-deficient (■) and wild-type (□) mice,  $n = 3$ . (C) Human apoptotic PMNs were instilled into the lungs of LPS treated mice; the numbers of recovered cells by BAL were counted ( $P = 0.0096$ ) and (D) phagocytic index was calculated ( $P = 0.0029$ ). Values reported are the mean  $\pm$  SE from 12 animals in each group. (E) CD44-deficient mice generate decreased concentrations of active TGF- $\beta_1$ . TGF- $\beta_1$  was measured in 10-fold concentrated BAL fluids, combined from four different wild-type (□) and CD44-deficient mice (■) at each time point,  $n = 3$ . Results are mean  $\pm$  SE from three experiments. Active TGF- $\beta_1$  is shown in the left panel and total TGF- $\beta_1$  in the right panel.

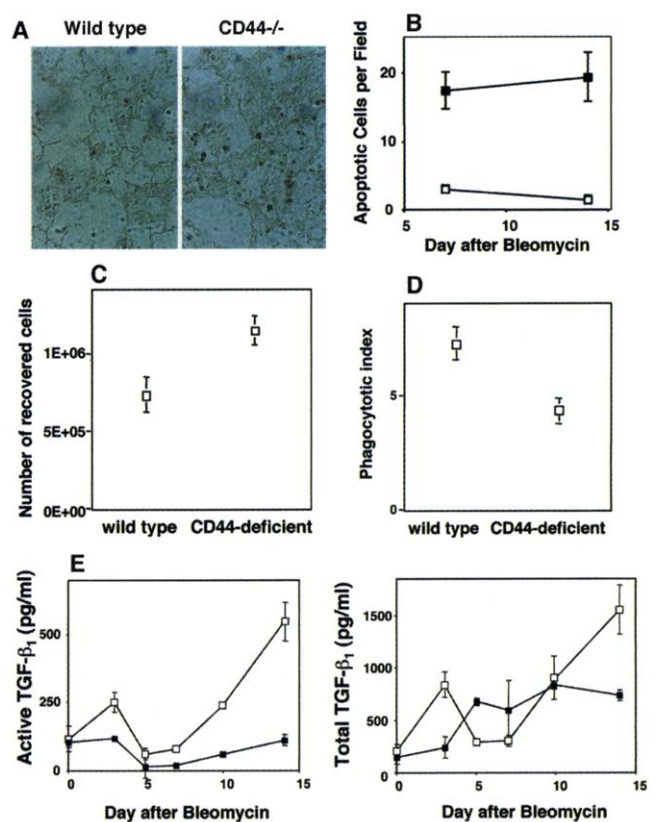
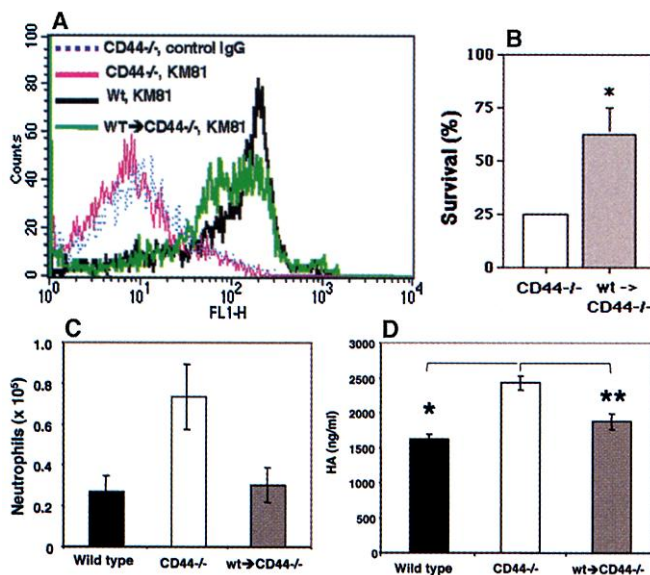


**Fig. 4.** Reversal of inflammatory phenotype by reconstituting CD44-deficient mice. (A) CD44<sup>+</sup> alveolar macrophages recruited to the lung after LPS challenge of CD44-deficient mice reconstituted with CD44<sup>+</sup> bone marrow (chimeric). (B) Survival at day 14 after bleomycin challenge in CD44-deficient and chimeric mice after reconstitution. Results are from two separate experiments with 10 mice in each group ( $P < 0.05$ ). (C) Neutrophil clearance at day 14 after bleomycin in wild-type, CD44-deficient, and chimeric mice after reconstitution. Results are from 10 mice in each group ( $P = 0.0269$ ). (D) HA clearance at day 14 after bleomycin in wild-type, CD44-deficient, and chimeric mice. Results are from 10 mice in each group. \* $P = 0.002$  between wild type and CD44<sup>-/-</sup>; \*\* $P = 0.0097$  between CD44<sup>-/-</sup> and chimeric mice; and  $P = 0.132$  between wild-type and chimeric mice.



with bone marrow from CD44<sup>+</sup> littermate controls (22). Successful reconstitution of CD44<sup>+</sup> alveolar macrophages and PMNs was demonstrated by fluorescence-activated cell sorting analysis of BAL cells from chimeric mice (Fig. 4A). Chimeric mice as well as reconstituted wild-type and CD44-deficient mice were challenged with intratracheal bleomycin and survival, inflammatory cell accumulation and HA content in BAL fluid were evaluated after 14 days. The survival defect and histologic changes in the lung tissue of the CD44-deficient animals after bleomycin treatment were significantly reversed by reconstitution with CD44<sup>+</sup> bone marrow (Fig. 4B). PMNs were cleared from the BAL fluid in both the wild-type and chimeric mice relative to the CD44-deficient mice (Fig. 4C). HA content was also reduced in the BAL fluid of the chimeric mice relative to the CD44-deficient mice (Fig. 4D). However, there was no significant difference in BAL fluid HA levels between wild type and chimeric mice suggesting that hematopoietic CD44 is the critical determinant of HA clearance after lung injury.

Previous studies have shown that CD44 is involved in recruiting T cells to inflammatory sites and regulates T cell-mediated endothelial injury (23, 24). Our results identify a previously unrecognized role for CD44 in resolving the inflammatory response following lung injury. CD44 deficiency leads to increased mortality from lung injury through unremitting inflammation characterized by accumulation of low-MW HA fragments, prolonged inflammatory gene expression, decreased clearance of apoptotic PMNs, and an impaired ability to generate active TGF- $\beta_1$ . Reconstitution of CD44<sup>+</sup>

alveolar cells partially reversed the phenotype demonstrating a requirement for CD44 in the successful resolution of the inflammatory response to tissue injury.

**References and Notes**

- V. A. Fadok et al., *J. Clin. Invest.* **101**, 890 (1998).
- J. S. Munger et al., *Cell* **96**, 319 (1999).
- A. Aruffo, I. Stamenkovic, M. Melnick, C. B. Underhill, B. Seed, *Cell* **61**, 1303 (1990).

- A. Bartolozzi, R. Peach, A. Aruffo, I. Stamenkovic, *J. Exp. Med.* **180**, 53 (1994).
- Q. Yu, B. P. Toole, I. Stamenkovic, *J. Exp. Med.* **186**, 1985 (1997).
- H. C. DeGrendele, P. Estess, M. H. Siegelman, *Science* **278**, 672 (1997).
- T. C. Laurent, J. R. Fraser, *FASEB J.* **6**, 2397 (1992).
- C. M. McKee et al., *J. Clin. Invest.* **98**, 2403 (1996).
- R. Schmits et al., *Blood* **90**, 2217 (1997).
- I. Y. R. Adamson, H. B. Drummond, *Am. J. Pathol.* **77**, 185 (1974).
- C. B. Underhill, H. A. Nguyen, M. Shizari, M. Culty, *Dev. Biol.* **155**, 324 (1993).
- M. M. Guo, J. E. Hildreth, *Anal. Biochem.* **233**, 216 (1996).
- J. D. McNeil, O. W. Wiebkin, W. H. Betts, L. G. Cleland, *Ann. Rheum. Dis.* **44**, 780 (1985).
- L. Roden et al., *Ciba Found. Symp.* **143**, 60 (1989).
- P. M. Sampson, C. L. Rochester, B. Freundlich, J. A. Elias, *J. Clin. Invest.* **90**, 1492 (1992).
- H. G. Lee, M. K. Cowman, *Anal. Biochem.* **219**, 278 (1994).
- S. P. Hart, G. J. Dougherty, C. Haslett, I. Dransfield, *J. Immunol.* **159**, 919 (1997).
- Apoptotic cells were detected in paraffin-embedded sections with DeadEnd Colorimetric Apoptosis Detection System (Promega, Madison, WI) following manufacturer's instructions.
- C. Haslett, L. A. Guthrie, M. M. Kopaniak, R. B. Johnston, P. M. Henson, *Am. J. Pathol.* **119**, 101 (1985), and (2).
- Q. Yu, I. Stamenkovic, *Genes Dev.* **14**, 163 (2000).
- Samples were analyzed with TGF- $\beta_1$  E<sub>max</sub> Immuno-Assay System (Promega, Madison, WI) following manufacturer's instructions.
- Six- to eight-week-old mice were irradiated with 1000 rads (<sup>137</sup>Cs radiador) followed by intravenous injection of 5 million bone marrow cells.
- H. C. DeGrendele, M. Kosfizer, P. Estess, M. H. Siegelman, *J. Immunol.* **159**, 2549 (1997).
- A. Q. Rafi-Janajreh et al., *J. Immunol.* **163**, 1619.
- Supported by a grant from the National Heart Lung and Blood Institute HL60539 (P.W.N.). P.T. was supported by the Swedish Heart Lung Foundation.

9 January 2002; accepted 4 March 2002

## Subnuclear Compartmentalization of Immunoglobulin Loci During Lymphocyte Development

Steven T. Kosak,<sup>1\*</sup> Jane A. Skok,<sup>3</sup> Kay L. Medina,<sup>1</sup> Roy Riblet,<sup>4</sup> Michelle M. Le Beau,<sup>2</sup> Amanda G. Fisher,<sup>3</sup> Harinder Singh<sup>1†</sup>

Immunoglobulin (Ig) loci are selectively activated for transcription and rearrangement during B lymphocyte development. Using fluorescence in situ hybridization, we show that Ig heavy (H) and Igk loci are preferentially positioned at the nuclear periphery in hematopoietic progenitors and pro-T cells but are centrally configured in pro-B nuclei. The inactive loci at the periphery do not associate with centromeric heterochromatin. Upon localization away from the nuclear periphery in pro-B cells, the IgH locus appears to undergo large-scale compaction. We suggest that subnuclear positioning represents a novel means of regulating transcription and recombination of IgH and Igk loci during lymphocyte development.

Constitutive heterochromatin and the nuclear periphery are the two major classes of transcriptionally repressive nuclear subcompartments. Evidence from studies in *Drosophila* and mammals suggests that the organization

of genes into heterochromatin may be one mechanism of regulated transcriptional repression (1-4). The role of the nuclear periphery as a repressive compartment has been well established in *Saccharomyces cerevi-*